Numerical simulation of the effect of cement particle shapes on capillary pore structures in hardened cement pastes

Cheng Liu [a, b], Guojian Liu [a], Zhiyong Liu [c], Lin Yang [d], Mingzhong Zhang [b], Yunsheng Zhang [a *]

[a] School of Materials Science and Engineering, Southeast University, Nanjing 211189, China

[b] Advanced and Innovative Materials (AIM) Group, Department of Civil, Environmental and Geomatic Engineering, University College London, London WC1E 6BT, UK

[c] Jiangsu Key Laboratory for Construction Materials, Southeast University, Nanjing 211189, China

[d] New Building Materials and Structures Research Centre, Zhengzhou University, Zhengzhou 450002, China

Abstract

Cement powder shapes have a pivotal role in particle packing and microstructural development, while its effect on capillary pore structure formation in three-dimension has not been fully understood. In this study, the modified CEMHYD3D model building on previous work of irregular-shaped cement particles is firstly used to simulate the evolution of capillary pore structures in cement pastes at various water-to-cement ratios. Pore networks at different curing time and degree of hydration are extracted and visualized. Subsequently, some home-made programs for determining three-dimensional pore structure characteristics including porosity, pore size distribution, pore connectivity and pore tortuosity are carried out on these simulated pore network extractions in hardened cement pastes. The results indicate that shape-induced larger surface area in more non-equiaxed irregular-shaped cement particles can improve pore structure parameters in hardened cement pastes, but this effect will be slight in the later curing period and at a low water-to-cement ratio. In addition, the less considered geometric difference plays a role in pore structure evolution especially for extremely non-equiaxed cement particle. However, the geometric attribute has a weak effect on pore structure parameters overall. It can also be concluded that the pore-to-solid ratio is still the most pronounced influence factor for pore structure parameters in hardened cement pastes.

Key words**:** modelling; cement particle shape; cement hydration; capillary pore; microstructure

1. Introduction

The network of pore structure of cement paste is crucial to mass transport properties in cement-based materials, which is usually considered as indicators to assess the durability and predict the service life of reinforced concrete structures[1, 2]. Different from traditional porous materials consisting of agglomerated particles, e.g., ceramics and metals, the topology of pore structure in cement-based materials is much more complicated due to the multiscale nature of microstructure and evolution of microstructure as a result of continuous hydration of cement. Pores in cement-based materials can be mainly classified into capillary pores and gel pores without a fixed critical threshold [3, 4]. As cement hydration proceeds, pore space between cement particles is gradually filled by hydration products, which leads to a refinement of capillary pore structure. By contrast, the increasing C-S-H containing gel pores can result in the formation of gel pore structure with its comparatively stable intrinsic attribute of structure [5]. Compared to small and tortuous gel pores, changeable capillary pore structure plays a decisive role in transport properties in cement-based materials [6]. Therefore, understanding the nature of capillary pore structure is of significance for investigating durability performance in cement-based materials.

It has been proved that pore structures in sintering porous materials, e.g., pore size distribution and pore tortuosity are strongly governed by performance of starting powders [7]. Particle shape, which is an important fact to be considered in starting powder, strongly influences properties of porous materials. In terms of cement-based materials, the evolution of capillary pore structure is highly dependent on cement hydration process and microstructural development. Many authors have focused on the experimental investigation of effects of raw material performance on pore structures in hardened cement pastes [8-10]. Although numerous studies concentrated on the effects of fineness (surface area) [8, 9] and chemo-activity [10] of raw materials, to the authors' best knowledge, that of particle shapes on pore structures has not been yet fully explored. This is attributed to that there is no effective technique for manipulating shapes of cement particles during production process in cement industry until now. In addition, the properties of cement powder, e.g., specific surface area and particle shape, are interacted during grinding process, which is impossible to isolate the effects of specific variables in experimental investigation. Fortunately, numerical simulation may provide an alternative way to investigate the particle shaped effects on capillary pore structures in hardened cement pastes.

Before performing analysis on pore structure in hardened cement pastes using numerical simulation, the primary conundrums are to determine shaped attributes of cement particles and achieve corresponding 3D hardened cement pastes. In recent years, the sophisticated X-ray computed tomograph (X-CT) using synchrotron sources for 3D imaging with high resolution of around 1.0 μm/voxel has been employed to capture shapes of cement particles combined with spherical harmonic functions [11, 12]. The reconstructed cement particles are then successfully coupled into discrete-based hydration model to simulate hydration process of this real cement [13, 14]. However, the resolution of 1.0 μm/voxel is still too limited for the majority of cement particle sizes, which can well reconstruct large particles with size of over 20 μm [12]. To overcome the limitation of resolution, a locally destructive technique named focused ion beam-tomograph (FIB-t) technique with even resolution of 15 nm/voxel has been used to determine shapes of cement particles of below 10 μm [15]. The 3D cement particles are reconstructed using stacks of successive images acquired from depth profiles in FIB-t based on electron microscopy imaging and nanoscale serial sectioning provided by focused ion beam. However, as the precision of spacing between the images is difficult to control in FIB-t, it is virtually impossible to reconstruct voxel-based 3D real cement particles, which will decrease accuracy of shaped reconstruction later. Moreover, reconstructed particle library from either X-CT or FIB-t is only available for a specific reference cement due to the complex, time-consuming and prohibitive experiments.

Alternatively, modelling regular-shaped particles including spherical particles [16, 17], ellipsoidal particles [18] and Platonic particles [19] are packed to represent fresh cement paste. Unfortunately, the over simplified regular-shaped particles of modelling real irregular-shaped cement unavoidably ignore the effects of shaped discrepancy on hydration in real hydrated microstructure. Furthermore, for the ellipsoidal and Platonic cement particles, the packing properties of pre-hydration microstructure can be analysed, while dynamic information in hydrated microstructure is not included. This is ascribed to that there is no approach in vector-based cement hydration model to extend spherical particles to other shaped ones for simulating microstructural evolution, e.g., HYMOSTRUC3D [16] and μic [17]. As such, it becomes more and more important to building cement hydration model based on irregular-shaped particles before investigating corresponding pore structures. Recently, our study [20] has reconstructed irregular-shaped cement particles library using central growth method on the basis of cellular automaton; these irregular-shaped particles are subsequently incorporated into discrete-based cement hydration model to investigate shaped effects on cement hydration process. The numerical simulation demonstrated that particle shapes have great influences on cement hydration: particle shaped discrepancy can not only affect cement hydration kinetics but determine setting behaviour of cement pastes. Therefore, this strong effect of cement particle shapes on hydration process leads us to consider whether cement powder shape has influence on capillary pore structure in hardened cement pastes.

This study aims at understanding the detailed relationship between cement particle shapes and pore structures in hardened cement pastes based on previously proposed cement hydration model using irregular-shaped particles. Firstly, the 3D microstructures of cement pastes are simulated using CEMHYD3D model based on different irregular-shaped cement particles generated using central growth model. The mechanism of central growth model is simply reviewed and detailed simulated cases are described in this section. Subsequently, some numerical methods for determining 3D pore structure parameters including porosity, pore size distribution, pore connectivity and pore tortuosity along with home-made programs are described in detail. Finally, the obtained pore structure parameters in cement pastes consisting of different shaped cement particles are analysed and compared to each other at water-to-cement ratios of 0.3, 0.4 and 0.5 with and without considering cement hydration kinetics.

2. Modelling of microstructural development

To directly analyse particle shaped effects on capillary pore structures, 3D microstructures of hydrating cement pastes made up of various shaped cement particles should be simulated. Our previous work has successfully proposed a 3D cement hydration model using irregular-shaped particles. This section will simply review its modelling principles and introduce some modifications in the latest version.

2.1. Irregular-shaped particle library

Different irregular-shaped cement particles can be reconstructed using a discrete-based method named central growth method. In the discrete-based method, all particles consist of a large number of fundamental voxels and their quality of reconstructed shapes is in turn controlled by the number of voxels. The core in central growth method is the growth eigenvector library which has direct relationship with particle shaped library. The relationship between one set of growth eigenvector and one certain particle shape is one-to-one correspondence. One mature particle can be obtained by voxel growth around one central voxel in a certain discrete growing space. In the growing space, the growth form is manipulated by the growth eigenvector. The value magnitude in each set of shaped eigenvector (between 0 and 100) represents growing probability around the growing point in the corresponding direction.

Fig. 1 illustrates a case of 2D evolution rules of central growth method in detail. In discrete growing space, the initial growing point is selected to be its central pixel and a certain set of growing eigenvector is also determined in advance, e.g., (9,78,29,61,14,60,25,67) in this case. Subsequently, if neighbouring pixels centred on the growth point are vacant, vacant pixels around initial central pixel are activated, e.g., eight marked neighbouring pixels shown in Fig. 1a. Accordingly, the values in eigenvector belonging to corresponding neighbouring pixels are compared to random numbers generated using the Monte Carlo simulation in turn. If the value in growing eigenvector is larger than the random number, the vacant pixel in according position turns to be a particle pixel. In this process, five vacant pixels of eight neighbouring ones are transformed into particle pixels, as marked pixels with numbers in Fig. 1b. Subsequently, these newly introduced particle pixels will become growing points in turn in the next iteration. In the next iteration, the pixel marked 1 becomes the growth point and its neighbouring pixels are also activated, as shown in Fig.1c. The corresponding values in growing eigenvector are then compared to randomly generated number belonging to according vacant neighbouring pixels. In this procedure, two vacant neighbouring pixels are transformed into particle pixels, shown in Fig. 1d. The above mentioned growing process is repeated, shown in Fig. 1e to Fig. 1h, until the surface area is satisfied with default value. From a large number of attempts, the shapes of particles generated using every set of default value have self-similarity with similar orientation under the condition of sufficient consisting pixels. As such, the shaped descriptors, specific surface area and three dimensions of the equivalent inertia ellipsoid, are employed to build shaped library for distinguishing different particle shapes.

In order to acquire particle with random orientation, the grown particle should be rotated by a random angle. Fig. 2 presents a case of one particle revolving an angle of 30°. During the rotation process in Fig. 2b, the phenomenon of "sieve holes" occurs unavoidably, which is pretty common in the discrete-based model [21]. The solution to this deficiency presented in Fig. 2c is the application of Boolean operations for eliminating holes in the interior of this particle. The above detailed information can refer to our recently published work [20].

Although the previous model can reconstruct different irregular-shaped particles, some defects still coexist. The most obvious defect is that some surficial pixels in grown particle may be isolated, as blue marked in Fig. 2h. In discrete model, there are three kinds of relationships between adjacent voxels in 3D, namely face-to-face, edge-to-edge and point-to-point neighbour model shown in Fig. 3. Normally, voxels in face-to-face neighbour model are regarded to be an integral part in the majority of cases [6, 22-24]. However, this work adopts the edge-to-edge neighbour model as a growing unit for improving growing efficiency, which leads to the occurrence of isolated voxel in the particle surface. Meanwhile, when implementing operation of eliminating "sieve holes", the previous model ignores the difference of constituent voxels between initial and terminal particles. This may results in particle volume instability. In order to overcome these defects, a technique of rearrangement of surficial voxels is proposed. The modified procedures are as follows. As the step of Boolean operations is carried out, these surficial voxels sharing edge or point with bulk particle voxels are erased from this grown particle. Subsequently, the remaining voxels are added in vacant space in the vicinity of particle surface until the volume difference disappears. The subsequence of location of filled vacant voxel follows from large area vacant pixel to small one. For example, the vacant pixel sharing three faces with particle surface in 2D (white marked in Fig. 1h) is firstly filled. After these modified procedures are completed, a comparatively perfect irregular-shaped particle can be achieved.

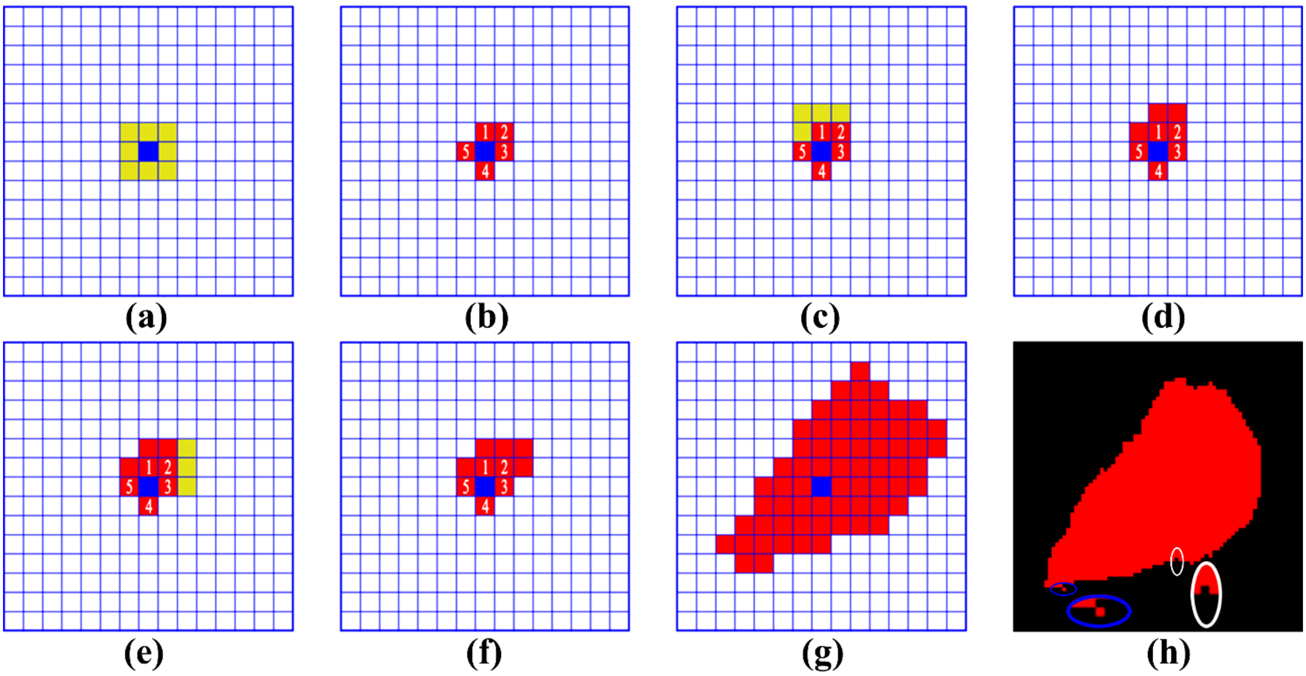

Fig. 1. Schematic of central growth method for generating irregular-shaped cement particles.

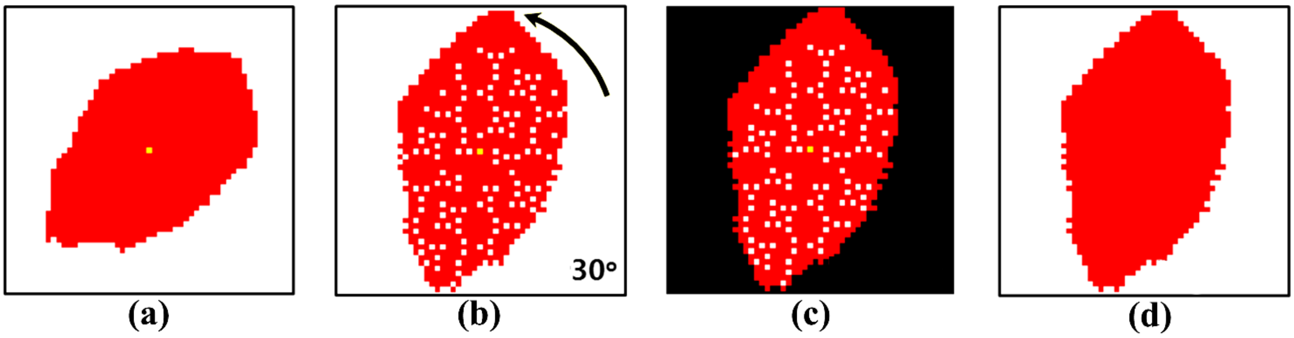

Fig. 2. Flow chart of rotating process and eliminating “sieve holes”.

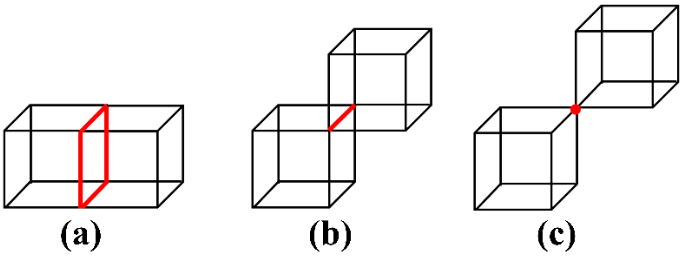

Fig. 3. Configuration of relationships between adjacent voxels: (a) face-to-face neighbour model; (b) edge-to-edge neighbour model; (c) point-to-point neighbour model

2.2. Simulated hydrated cement pastes

The pre-hydrated cement pastes consisting of four representative shaped cement particles are respectively incorporated into CEMHYD3D model to simulate hydration process. Four representative shapes are named spherical, flat, intermediate and elongated shapes with three dimension ratios of the equivalent inertia ellipsoid of 1.10:1.08:1.00, 1.43:1.21:1.00; 2.04:1.50:1.00 and 3.11:1.27:1.00 respectively, as shown in Fig. 4. Each shaped cement particle makes up one packing pre-hydration microstructure for comparison of shaped effect on capillary pore structure. In this study, the representative volume element (RVE) is chosen to be a cubic volume of 100 μm on each side with resolution of 0.5 μm/voxel. This is attributed to that the simulated cement paste in the size of 100 μm has representation and irregular-shaped particles based on central growth method can well be reconstructed with high volume stability in resolution of 0.5 μm/voxel. The reconstructed irregular-shaped particles are packed into RVE using periodic boundary conditions and following the sequence from the large particle to the small one. The input parameters of cement including particle size distribution, mineral phase distribution and mineral phase content in cement powder are in accordance with a Chinese Portland cement named P.I cement (similar to the ASTM Type I

Portland cement). The mineral phase compositions of Type I cement obtained from BSE-EDS image are 52.36% C_3S, 29.75% C_2S, 4.77% C_3A and 13.12% C_4AF respectively. The specific surface area of this cement powders is 465.8 m^2/kg obtained from laser particle size analyser. The detailed input parameters of Type I cement can refer to Ref. [20].

Cement hydration processes of water-to-cement (w/c) ratios of 0.3, 0.4 and 0.5 are simulated and determined. A case of pre-hydrated microstructures packed using spherical, flat-, intermediate- and elongated-shaped cement particles at w/c=0.4 is shown in Fig. 4. In CEMHYD3D model, modelling hydration is carried out via cycles of dissolution, diffusion and reaction according to known reaction equations of mineral phases. The relationship between computational cycle (n) and real time (t) is satisfied with equation of parabolic hydration kinetics

$$t = \beta n^2 \qquad (1)$$

In terms of curing conditions, saturated condition is simulated in which water content in capillary pores keeps saturated before capillary pores are totally disconnected. As capillary pores reach the totally disconnected state, the curing condition is automatically switched to the seal condition in which the consumed water by hydration is not replenished. This is ascribed to the fact that the experimental hydration properties in the saturated condition is employed to calibrate simulated ones previously, which can be related to the real hydration process. The curing temperature is constant at 20 °C for all cement pastes, which is consistent with the experimental condition [20].

Noticeably, there are two assumptions for simulated microstructural evolution of cement pastes. In the early age for cement pastes, the surface area of initial cement particles is the dominant factor to influence hydration process [25]. As such, the first assumption is that the simulated hydration process of pre-hydrated microstructure with same surface area as real cement powders can show consistency with real cement hydration process. Herein, the simulated hydration process of intermediate-shaped cement particles is utilized to fit experimental hydration process of Type I cement. In the initial CEMHYD3D model using digitalized spheres as cement particles the value of conversion factor β is calibrated to be close to a constant in simulated cement pastes at different w/c ratios [26] or with different cement fineness [27]. More importantly, the experimental validation of hydration preocess in simulated cement pastes is impossible to be obtained for specific shaped particles. Therefore, β is subsequently supposed to be a constant value for all simulations with different shaped particles. Although conversion factors β in different microstructures generated using different shaped cement particles are various as calibrated with the experiment data regardless of the shaped discrepancy (this case is also included in this study), surface area difference should be yet included for comparison of the effects on hydration kinetics. Meanwhile, the meaning of conversion factor β in Eq. (1) has no rational interpretation until now [13, 26]. As such, these assumptions are reasonable as considering the effect of surface area of particles on cement hydration. As calibrated using measured hydration properties, the value of β is 0.000096 h/cycle^2 for all simulations. During continuous monitoring of cement hydration process, microstructures consisting of different shaped particles are extracted at curing time of 0, 1, 7 and 28 days. On the other hand, to eliminate effect of hydration kinetics, typical microstructures with same degree of hydrations of 0, 0.2, 0.4, 0.6 and 0.8 are also extracted. After obtaining simulated cement pastes, some home-made programs for quantitatively determining pore structure parameters are performed on these microstructures, which will be discussed in Section 3.

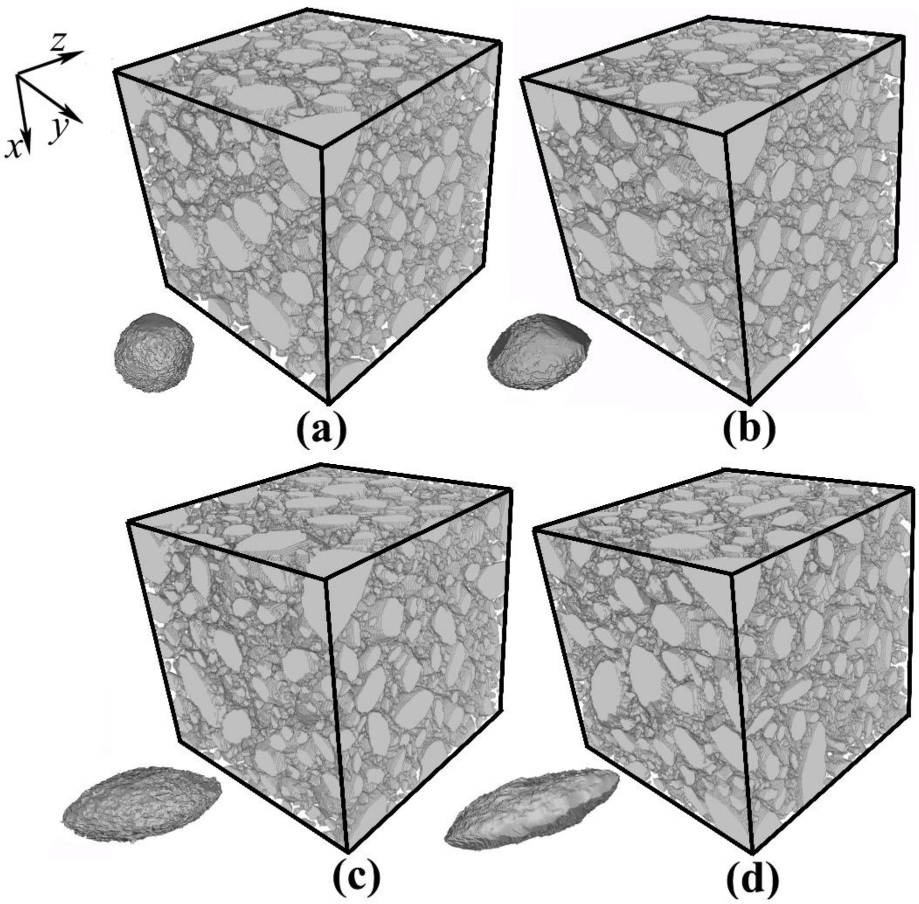

Fig. 4. Schematic of pre-hydrated microstructures generated using (a) spherical, (b) flat-, (c) intermediate- and (d) elongated-shaped cement particles at the w/c ratio of 0.4.

3. Modelling of capillary pore structure characteristics

As the obtained microstructures of cement pastes are comprised of discrete cubic elements, all home-made programs of quantitatively determining pore structure parameters including porosity, pore size distribution, pore connectivity and pore tortuosity are voxel-based. In discrete-based model, the resolution-related problem induced by the limitation of experimental measurement or calculation ability is unavoidable and widely-investigated [28-31]. However, this problem is out of the scope of this study. To validly compare the effect of cement particle shapes on capillary pore structures, the same resolution (0.5 μm/voxel) is employed for all simulated microstructures. In addition to the resolution-induced limitation, the analysis procedure of pore texture for voxel-based microstructure strongly depends on the selected adjacent neighbour model [31] shown in Fig. 3. Consequently, in accordance with the overwhelming majority of studies of pore structure, face-to-face neighbour model is selected for all 3D discrete capillary pore structures.

3.1. Porosity

In the 3D voxel-based microstructure, pore and solid phase can be labelled respectively and pore structure should also be extracted from the microstructure. The pore voxel can be determined by point-to-point scanning. Porosity (*P*) is obtained following the equation

$$P = \frac{V_p}{V_b} \qquad (2)$$

where V_p and V_b are pore volume and bulk volume of the cement paste respectively.

3.2. Pore size distribution

It has been proved that pore size distribution (PSD) correlates with the related properties in cement-based materials, e.g., transport properties [32-34], while there are numerous PSD definitions based on different experimental measurements and modelling methods. On the basis of different mathematical definitions PSD can be classified into discrete PSD and continuous PSD [35]. This study aims at investigating particle shaped effects on pore structures in cement pastes rather than focuses on comparison between different PSD definitions. Therefore, a discrete PSD named 3D voxel-erosion method alongside a home-made program is proposed to achieve PSDs in microstructures generated using different shaped particles [6]. In this method shown in Fig. 5, voxels in each 2D section are firstly labelled to be solid and capillary pore phase based on their occupancy. Subsequently, pore voxels sharing at least one face with a solid voxel are marked with number 1. In the next step, pore voxels sharing at least one face with the voxels labelled 1 are labelled 2. The same process is iterated until all pore voxels are marked with the number of steps required to erode them from the pore-solid boundaries. The maximum number of steps in each isolated pore in 2D is the radius of this pore in voxel-unit. This algorithm is successively employed on each 2D section. Finally, combined with the resolution in the digital structure, PSD can be determined. Although voxel-erosion method is one of many possible definitions of pore size and ignores the information regarding pore-topology, e.g., connected and disconnected pores, it can quickly get relative results of PSDs in discrete cement paste microstructures.

Due to local heterogeneity in the cubic shaped RVE [22], the modelling PSDs in different directions using this method may exist local difference. The PSDs in different directions of unhydrated cement paste RVE with a w/c ratio of 0.4 are shown in Fig 6(a). It can be seen that the PSDs in different directions of RVE shows a weak difference. Meanwhile, the difference of PSDs is greater as the spherical cement particle is replaced by an elongated-shaped one. In order to overcome this drawback, an average PSD in three different directions of RVE can be used to evaluate the effect of shapes of cement particle on PSD of cement pastes. Correspondingly, the average PSDs of unhydrated cement pastes consisting of spherical and elongated-shaped cement particles are shown in Fig. 6(b). It can be found that the difference of PSDs between different shaped cement particles is observed to be pronounced. Therefore, the overage PSD in three direction of cubic RVE is employed to represent overall PSD in this study.

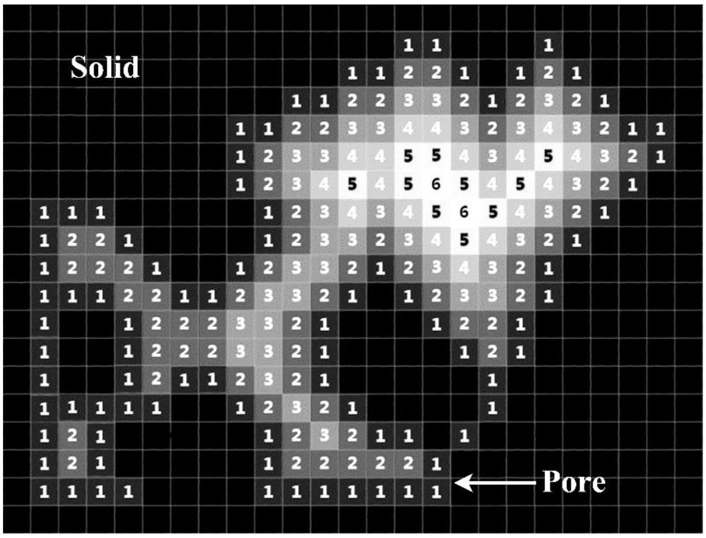

Fig. 5. Definition of pore size. Solid phase is black pixels and pores are grey pixels marked with numbers denoting the step number required to erode from the closest solid phase pixel.

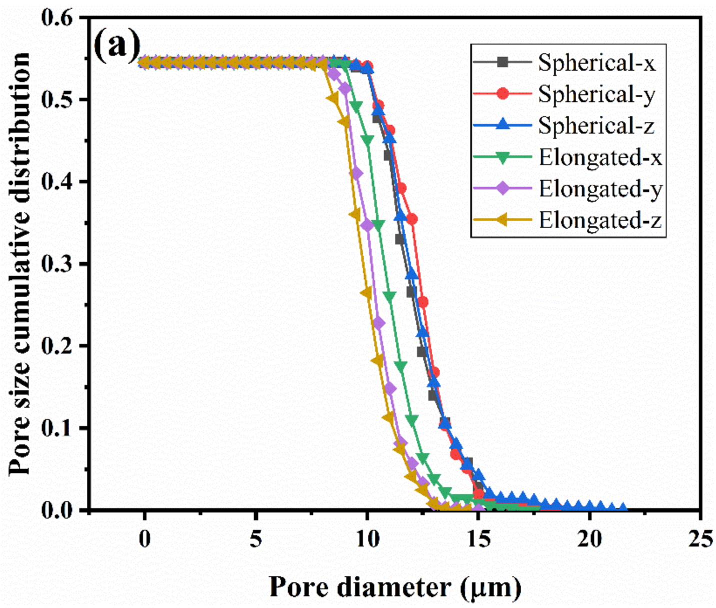

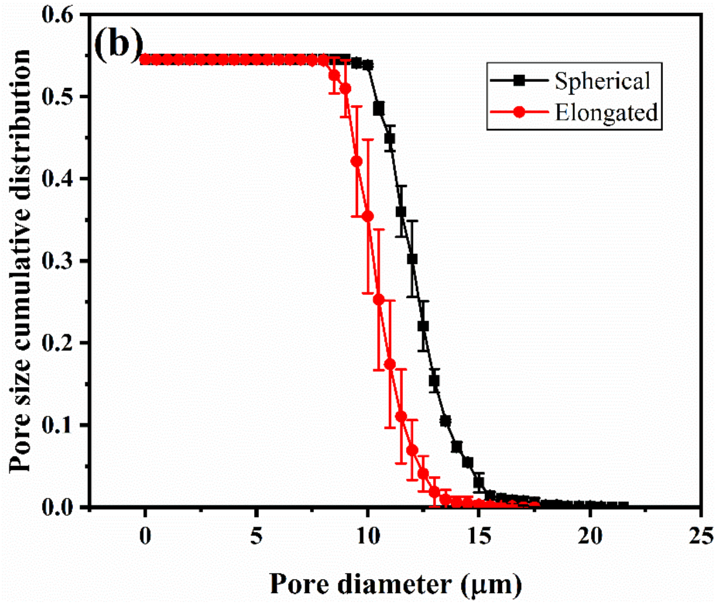

Fig. 6. An example of pore size distributions in unhydrated cement pastes consisting of spherical and elongated-shaped cement particles with a w/c ratio of 0.4. (a) PSDs in different directions of cubic RVE; (b) the average PSD.

3.3. Pore connectivity

Capillary pore connectivity is one of the most important characteristics for pore structure in cement-based materials, which directly controls transport properties. Through connected capillary pore network, harmful species can migrate freely from external environment to the depth of cement-based materials. To quantitatively characterize capillary pore depercolation process in microstructural evolution, the well-known “burning algorithm” [23, 24] combined with face-to-face neighbor model shown in Fig. 7 is employed. In the voxel-based microstructure, the first pore voxel of surface slice in RVE chosen as burning point is burnt; the pore voxels contacting this burning point are accordingly burnt, by that analogy, until all connected pore voxels in this pore cluster containing the first burning point are burnt. Based on face-to-face neighbor model, if two pore voxels contact by face-to-face form in 3D, these two pore voxels are connected, while two pore voxels contact by other two forms, edge-to-edge and point-to-point form, these two are disconnected. If the pore voxels can be burnt from one surface to the opposite surface, this pore cluster is connected. In order to model cement hydration in infinite field, periodic boundary conditions are employed in this RVE, mentioned in Section 2.2. As a result, connectivity in boundary surfaces should also be considered. In this study, only pore clusters with connected pores in two surface slices are determined to be connected. Following this process, all connected pore clusters can be detected, e.g., pores of labelled 1 and 2 in Fig. 7.

Some importance should be attached to the remaining pores classified into isolated pores and dead end pores shown in Fig 7. In cement-based materials, transport properties, e.g., diffusivity, strongly depend on capillary pores and porous C-S-H. For example, the average diffusion coefficient in porous C-S-H is much smaller than that in capillary pores, normally with two to four orders of magnitude difference [6]. Due to great difference of diffusion properties in capillary pores and C-S-H, the improvement of ion diffusion in isolated pores for overall diffusivity in cement pastes should be slight. By contrast, dead end pores still play a crucial role in diffusion properties in cement pastes in spite of with disconnected attributes. Although dead end pores cannot traverse cement paste matrix, they yet serve as quick access for harmful ions from external environment. Ions can easily diffuse into the depth of cement pastes. However, investigation of shaped effects on dead end pore morphology is not included in this work.

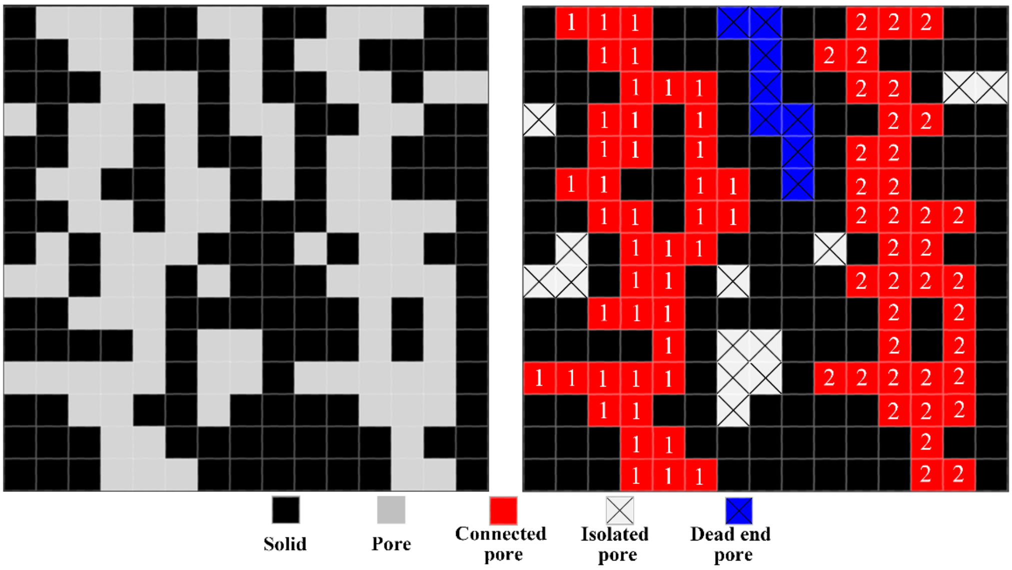

Fig. 7. Schematic illustration of pore types and burning algorithm.

3.4. Pore tortuosity

Among these capillary pore structure parameters, numerous studies [28, 36, 37] have attached great importance to tortuosity in cement paste 3D microstructure for understanding aggressive species transport process in capillary pores. In porous materials, the classic definition of tortuosity (τ_G) is given as a ratio of “effective average path”, $<L_e>$, of a fluid (or an electric) particle to the corresponding straight and shortest distance, L, along the direction of macroscopic flux [38]. This tortuosity is defined as geometric tortuosity. In some literatures, to characterise the average tortuosity in porous materials, diffusion tortuosity (τ_D) is introduced to be defined as the ratio the self-diffusion coefficient (D_0) of non-sorbing species in the free space to the long-time self-diffusion coefficient (D_∞) of these species in pore space [38]. Nevertheless, these two concepts have the following relationship

$$\tau_G = \frac{< L_e >}{L} = \sqrt{\tau_D} = \sqrt{\frac{D_0}{D_\infty}} \qquad (3)$$

where geometric tortuosity just takes into account the proper power of diffusion tortuosity [28]. In diffusion tortuosity, the self-diffusion coefficient D in 3D space is defined using time derivatives of mean square displacement

$$D(t) = \frac{1}{6}\frac{d\left\langle l(t)^2 \right\rangle}{dt} \qquad (4)$$

where t is time and $<l(t)^2>$ is mean square displacement of random walker.

To quantitatively determine pore tortuosity in hardened cement paste, numerical simulation should be implemented on 3D microstructures. A range of voxel-based (or pixel-based) algorithms have been proposed to measure tortuosity in porous material structures including medial axis [39], Dijkstra algorithm [40], A-star algorithm [41] and fast marching method thin-line skeleton [42]. In this work, a 3D random walk simulation [28, 36, 37] of simulating self-diffusion behavior along with a home-made program is employed to compute tortuosity by the mean square displacement (MSD) of randomly walking "ants" in the percolating capillary pore voxels as a function of time. The programming mechanism is as follows: sufficient "ants" used to model diffusion specimen in pore structure migrate on the pore voxel selected randomly, as the start position of the lattice walk trial at integer time equals to 0. A trial move is performed with the space step of one voxel distance in one of the six possible directions. The ant then executes a random jump to one of the nearest pore voxels and the time of walk is incremented by one unit integer time after the jump. If the randomly chosen voxel is a non-pore phase, the ant will stay at previous location and the jump is not performed, while the time is still incremented by one unit. As time elapses, the ants will go out of the discrete RVE. This out-leaching phenomenon is undesirable and inevitable because of limited system size. As such, periodic boundary conditions on the 3D microstructures are employed to address this out-leaching problem, which is in accordance with previous performance. After an abundant number of walking steps (t) of sufficient ants (n), the diffusion tortuosity can be determined by the following equation:

$$\tau_D = \frac{\left\langle l_f^2(t) \right\rangle}{\left\langle l_{cp}^2(t) \right\rangle} \text{ as } t \to \infty \tag{5}$$

where $\left\langle l_f^2(t) \right\rangle$ and $\left\langle l_{cp}^2(t) \right\rangle$ are mean square displacement in free space and porous media respectively. The mean square displacement is satisfied with:

$$\left\langle l^2(t) \right\rangle = \frac{1}{n}\sum_{i=1}^{n}\left[\left(x_i(t)-x_i(0)\right)^2-\left(y_i(t)-y_i(0)\right)^2-\left(z_i(t)-z_i(0)\right)^2\right] \tag{6}$$

where $x_i(t)$, $y_i(t)$ and $z_i(t)$ are the coordinate of ant *i* at time *t*, and $x_i(0)$, $y_i(0)$ and $z_i(0)$ are the starting position of ant *i*.

Normally, pore structure in cement paste is often anisotropic. Equation (6) can further break down to discuss the tortuosity of anisotropic cement paste:

$$\left\langle x^2(t) \right\rangle = \frac{1}{n}\sum_{i=1}^{n}\left(x_i(t)-x_i(0)\right)^2 \tag{7}$$

$$\left\langle y^2(t) \right\rangle = \frac{1}{n}\sum_{i=1}^{n}\left(y_i(t)-y_i(0)\right)^2 \tag{8}$$

$$\left\langle z^2(t) \right\rangle = \frac{1}{n}\sum_{i=1}^{n}\left(z_i(t)-z_i(0)\right)^2 \tag{9}$$

Accordingly, the three dimensional tortuosity can be acquired by using each dimensional MSD to replace $<l^2(t)>$ in Equation (6). The MSD of 50000 ants in the free space without solids is shown in Fig. 8. The fitted slopes of $<x^2>$, $<y^2>$) and $<z^2>$ are all nearly 0.33 and that of $<l^2>$ is 1.00. This agrees well with the theoretically predicted results combined with Equation (5) to (9), namely the three dimensional MSD is equal to 1/3 total MSD in free space. This strongly demonstrates the modelling method is reasonable.

Because local heterogeneity of pore structure in hardened cement paste exists and the random walk simulation is a statistics-based method [43], the obtained tortuosity in hardened cement paste is highly dependent on the ant quantity and walk steps. To determine the reasonable values, different cases are carried on the capillary pore structure of unhydrated cement pastes consisting of spherical particles with a w/c ratio of 0.4. Firstly, the mean square displacements of different ant quantities against time of lattice walk are shown in Fig. 9. It can be found that as the number of ant is smaller than 5000, the predicting mean square displacement dramatically fluctuates with time of lattice walk increasing. However, the relationship between mean square displacement and time of lattice walk shows a strongly linear increase as the number of ant exceeds 5000, which means this number of ant is satisfied with the modelling demand. To increase the modelling precision combined with the consideration of computational demand, the quantity is selected to be 50000 for all cement paste microstructures in this study. After determining the ant quantity, the time of lattice walk should also be determined. The slope of the curve of mean square displace against time of lattice walk as function of time of lattice walk is shown in Fig. 10. It can be observed that as the number of time of lattice step exceeds 100000, the slope is almost kept at a constant value with around 0.71. It means the threshold of time of lattice walk is 100000. Similar to the rule to determine the ant quantity, the time of lattice walk is selected to be 1000000 for all cement paste microstructures. All above mentioned programs are performed by a single 64-bit PC (Intel(R) Core(TM) i7-6820HQ CPU @ 2.70 GHz, RAM memory 16 GB).

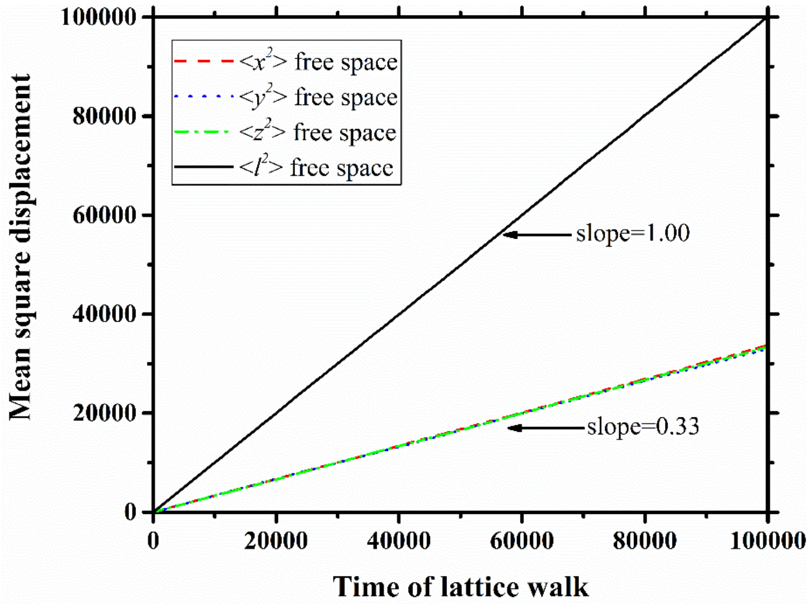

Fig. 8. Schematic of mean square displacement against time of lattice walk in 3D free RVE.

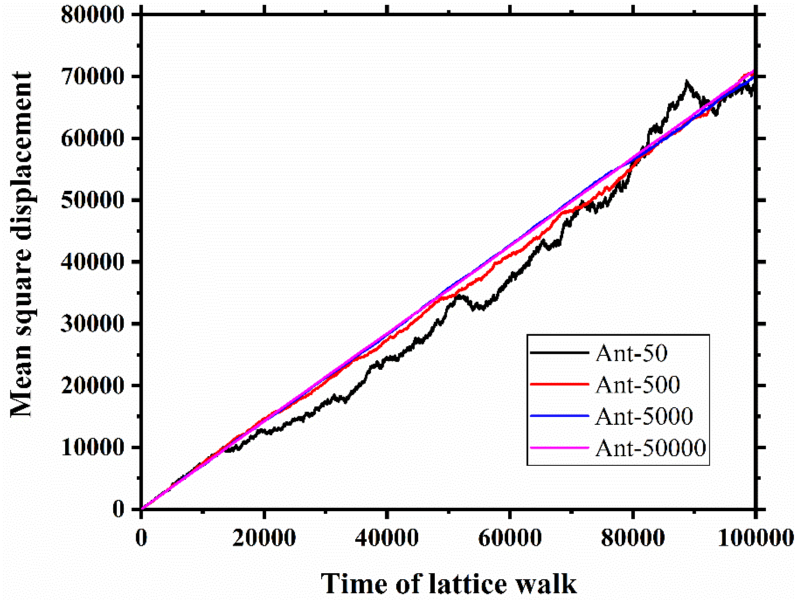

Fig. 9. Schematic of mean square displacement against time of lattice walk in unhydrated cement paste consisting of spherical particles with a w/c ratio of 0.4 using different ant quantities.

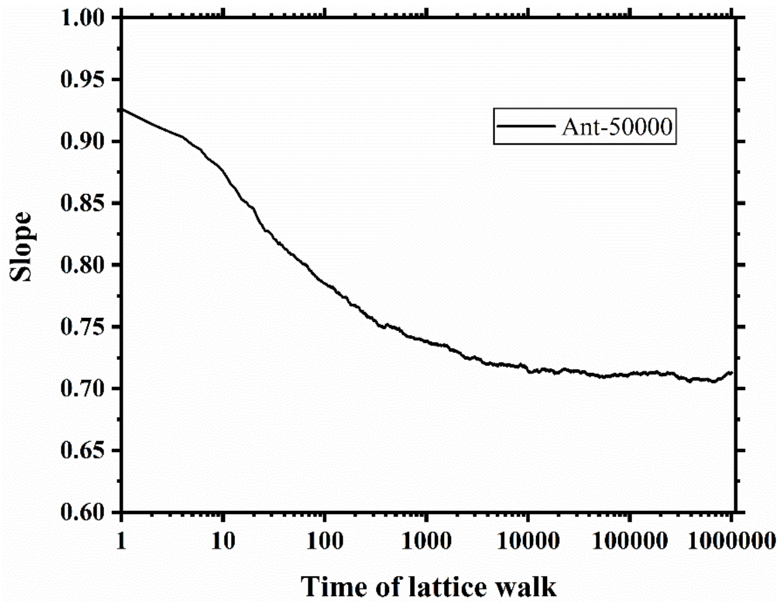

Fig. 10. Schematic of slope against time of lattice walk in unhydrated cement paste consisting of spherical particles with a w/c ratio of 0.4 using 50000 ants.

4. Results and discussion

4.1. Porosity

The evolution of capillary porosities in simulated hardened cement pastes consisting of different shaped cement particles is illustrated in Fig. 11. In all cement pastes regardless of particle shapes and w/c ratios, porosity evolutions show the similar changing tendency with time elapsing. In detail, porosities in cement pastes at the same w/c ratio decrease slightly in the early 10 h, then fall dramatically in the next 100 h, accounting for over 40% of initial porosities, finally reach a steady tendency after 100 h. In terms of the effect of the shaped discrepancy, cement pastes with elongated-shaped particles show the greatest decreasing tendency especially between 10 h and 100 h compared to other ones. At w/c ratios of 0.4 and 0.5, cement pastes consisting of elongated- and intermediate-shaped particles contain less capillary pores compared to that of spherical and flat-shaped particles. It means that the more non-equiaxed cement particle is, the much greater decrease of porosity it will have. It can be attributed to surface area difference in essence where cement particle with less equiaxed has larger surface area. Cement particles with large surface area can dramatically improve hydration rate in the early curing period.

However, the difference of porosity is disappeared in later curing period and at a low w/c ratio, e.g., cement pastes after curing time of 100 h at the w/c ratio of 0.3. This is ascribed to that water content at w/c=0.3 is not sufficient for cement to totally hydrate. Although cement consisting of spherical and flat-shaped particles is with low hydration rate, its hydration potential is the same as that consisting of high surface area particles. When the hydration rate of cement with high surface area is decreasing even stopped in the later period, one with low surface area can still hydrate due to the remaining considerable water content. It should be noticed that cement pastes made up of spherical particles shows the similar changing curve of porosity as that made up of flat-shaped particles in spite of with different shapes. This is attributed to that simulated discrete spherical shape with many local small protuberances in this study is not the perfect digitalized sphericity, which increases surface area of spherical particle. This leads to slight surface area difference between pre-hydration microstructure consisting of spherical and flat-shaped cement particles. As such, hydration kinetics affected by surface area in these two cement pastes show great similarity.

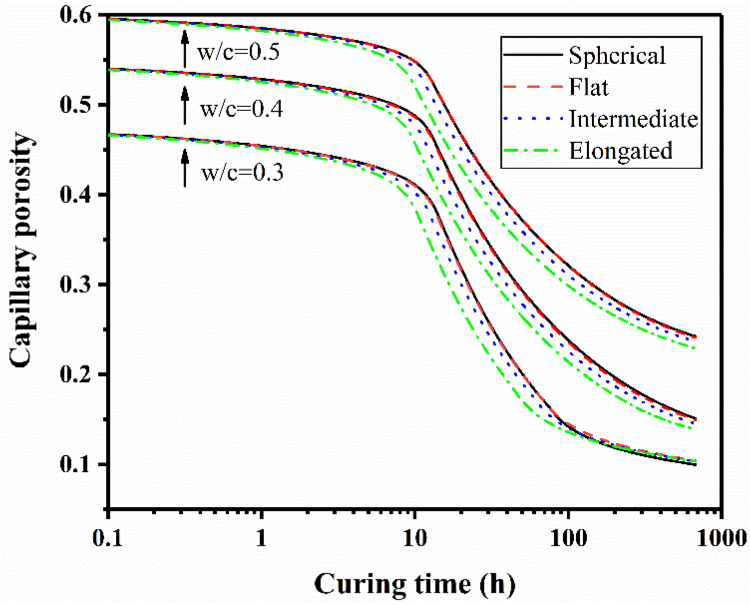

Fig. 11. Porosity in simulated cement pastes consisting of different shaped cement particles.

4.2. Pore size distribution

The program of 3D voxel-erosion method is performed on the networks extracted from simulated cement pastes microstructures at curing time of 0, 1, 7 and 28 d respectively. As shown in Fig. 12, the representative pore network extractions consisting of spherical and elongated-shaped cement particles at the w/c ratio of 0.4 are visualized. It can be found that initial pore clusters become smaller and some pore voxels extend to the locations where solid phase voxels occupy previously as cement hydration proceeds. Fig. 13 shows the effect of particle shapes on pore size distributions in cement pastes with different curing time at w/c=0.3, 0.4 and 0.5. It can be found that with cement hydration from 0 d to 28 d, pore sizes in cement pastes gradually decrease due to the fill of hydration products in capillary pores. Additionally, in accordance with the effect of particle shapes on porosity, the less equiaxed particles with higher surface area can lead to lower pore size in the hardened cement paste at early curing age, e.g., 1 d, because of higher hydration rate. However, this shaped effect on pore size will be decreasing after curing time of 1 d. The reason is that the effect of higher surface area resulting from initial particle shape will gradually retard with cement hydration, especially for the particle of less shaped difference, e.g., flat- and intermediate-shaped particles. In respect to the effect of the w/c ratio, the increasing w/c ratio can extend shaped effect on pore size in cement pastes, as shown in Fig. 13(c). At curing age of 1 d, the middle pore size in cement paste consisting of elongated-shaped particles at w/c=0.5 with around 7.5 μm is even only 0.5 time of that consisting of spherical particles. However, this difference of middle pore size is very slight for the same shaped cement pastes at w/c=0.3. Consequently, irregular-shaped particles with high surface area is beneficial to decreasing pore size in cement pastes, especially at a high w/c ratio.

In the previous studies, apart from surface area, the less considered geometric discrepancy of irregular shaped particles also has influence on cement hydration process. As a result, in order to eliminate kinetics in cement hydration process, the program for determining pore size distribution is also carried out on the networks at degree of hydrations (DoHs) of 0, 0.2, 0.4, 0.6 and 0.8. Fig. 14 shows the effect of particle shapes on pore size distribution with different degree of hydrations at w/c ratios of 0.3, 0.4 and 0.5. As can be seen from Fig. 14(a-c), particle shaped difference has great influence on pore size at early curing time for a high w/c ratio (0.5). For example, middle pore size in hardened cement pastes with the w/c ratio of 0.5 at DoH of 0.2 consisting of elongated-shaped particles is almost 2.0 μm which is much smaller than that consisting of spherical ones with around 8.0 μm at the same conditions. Nevertheless, this effect can be neglected for capillary pores in hardened cement pastes at high DoHs (0.6 and 0.8) for small w/c ratios (0.3 and 0.4). This can be ascribed to that non-equiaxed particles are beneficial to decreasing particle-to-particle spacing in packing system compared to equiaxed particles, e.g., spherical shape [18]. At the low DoH, the packing effect of initial non-equiaxed cement particles with local sharp surface regions are crucial to decreasing capillary pore size. However, the surficial shape of initial cement particle for non-equiaxed particle is gradually ambiguous and tends to be more spherical with cement hydration [13]. In addition, the geometry of hydration products as filled solids of capillary pores shows great disorder and randomness in the simulated hardened cement pastes. The geometric effect of cement particles becomes more and more ignorable at the high DoH. As such, geometric effect of cement particles has effect on pore size in cement pastes in the early period, while this effect will be slight for cement pastes with low w/c ratios and high DoH.

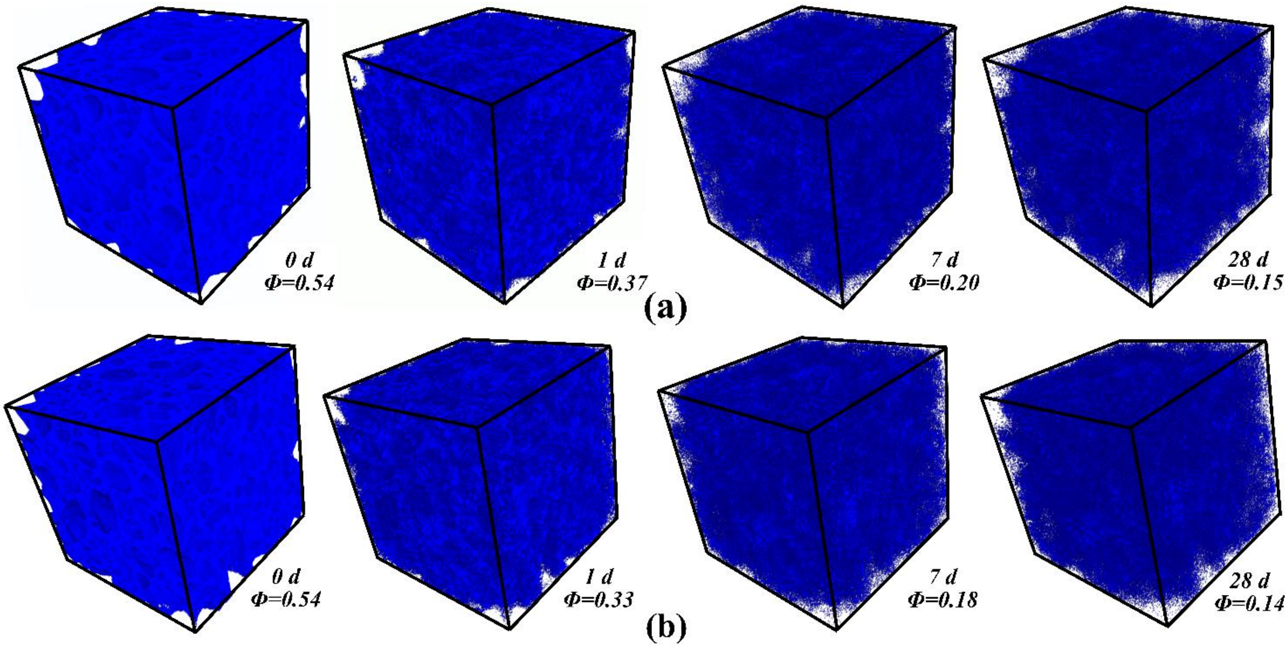

Fig. 12. 3D pore structures of hardened cement pastes at curing time of 0, 1, 7 and 28 d with the w/c ratio of 0.4.(a) spherical particles. (b) elongated-shaped particles . Φ means capillary porosity.

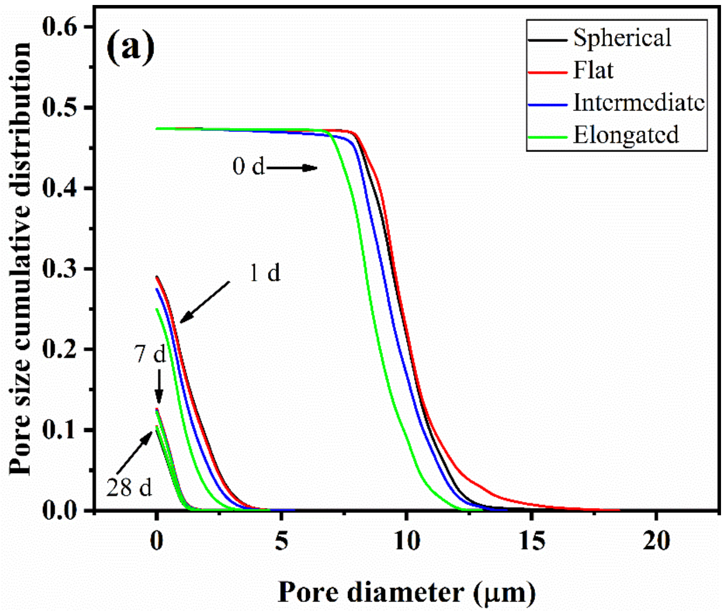

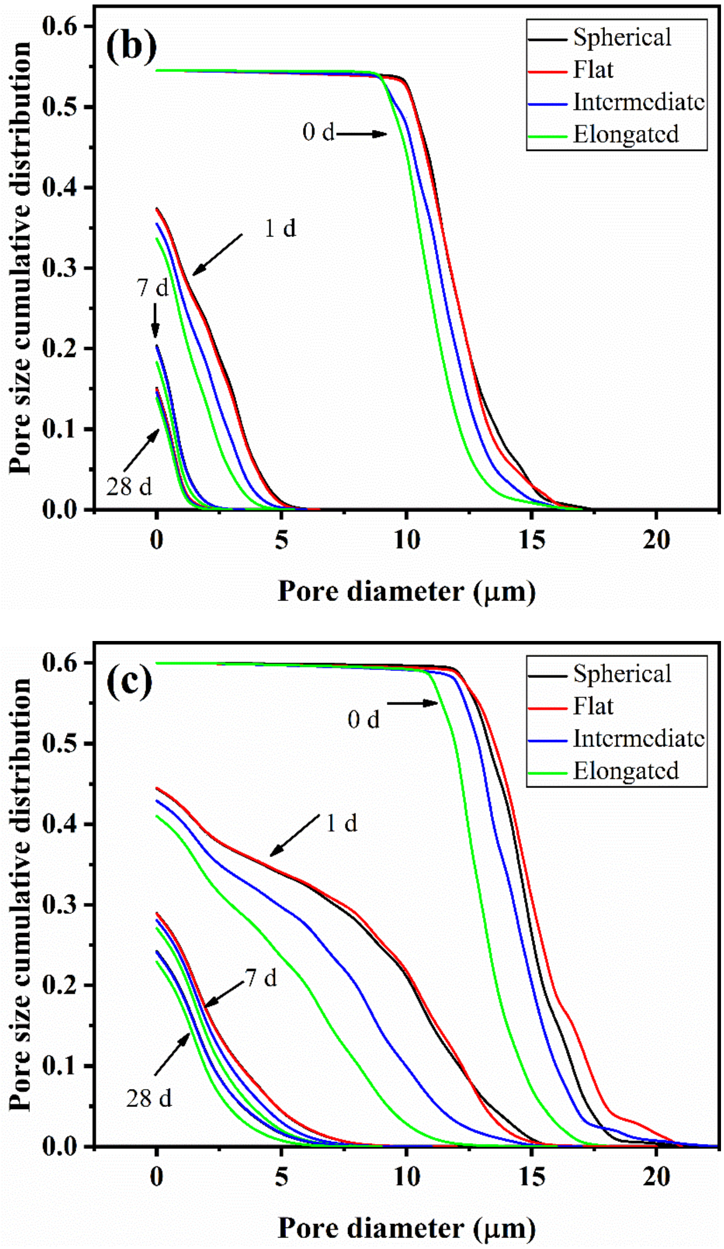

Fig. 13. Pore size distributions in simulated cement pastes with different curing time at w/c ratios of (a) 0.3 (b) 0.4 and (c) 0.5.

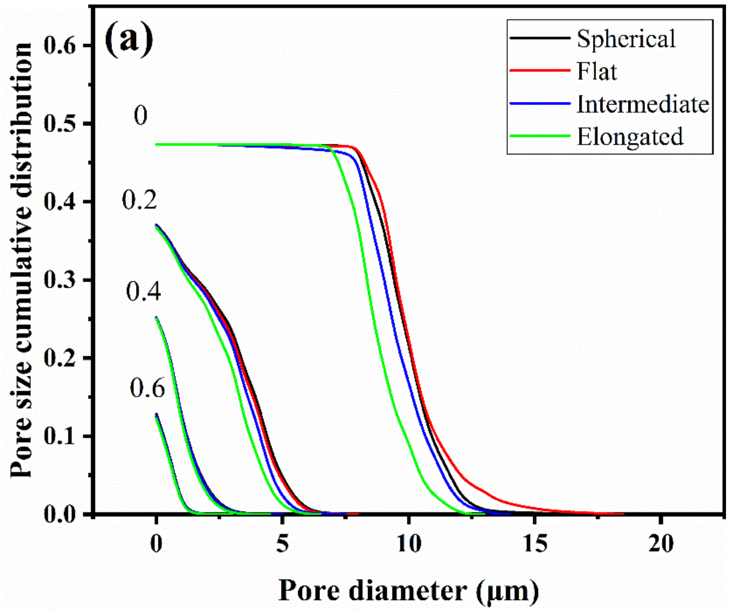
(a)
Spherical
Flat
Intermediate
Elongated
0
0.2
0.4
0.6
Pore size cumulative distribution
0.0
0.1
0.2
0.3
0.4
0.5
0.6
0
5
10
15
20
Pore diameter (μm)

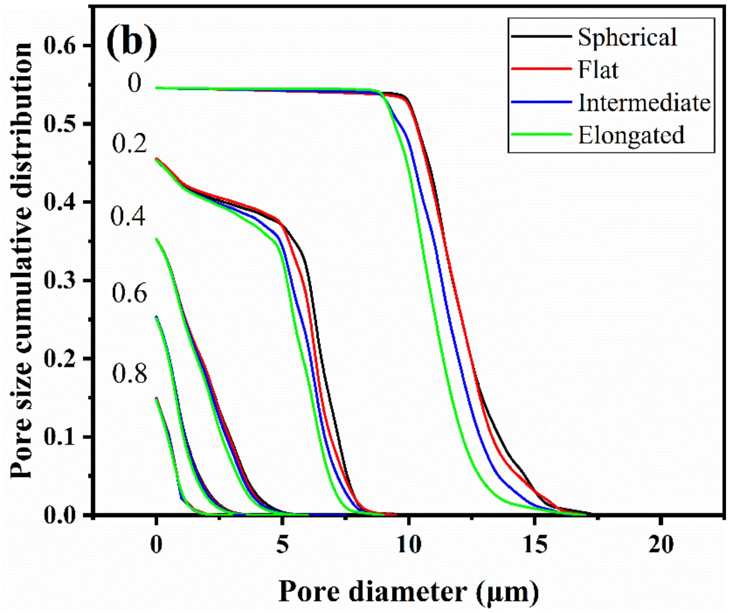
(b)
Spherical
Flat
Intermediate
Elongated
0
0.2
0.4
0.6
0.8
Pore size cumulative distribution
0.0
0.1
0.2
0.3
0.4
0.5
0.6
0
5
10
15
20
Pore diameter (μm)

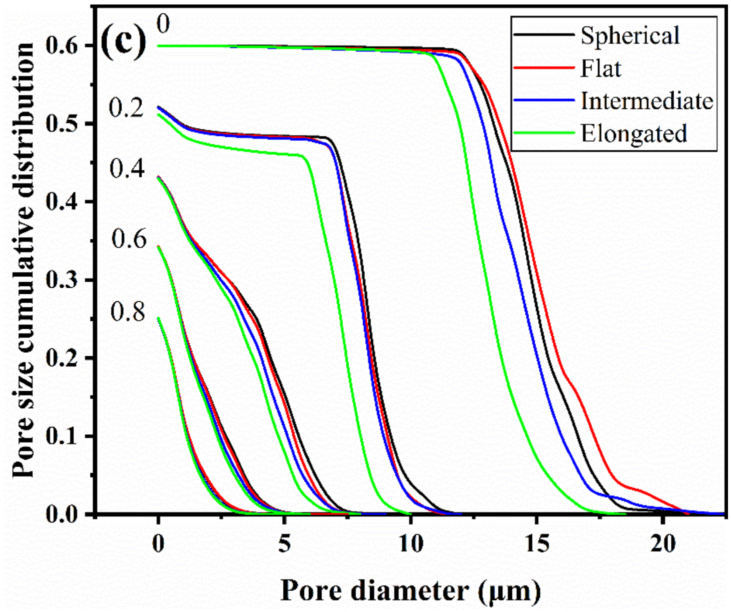

Fig. 14. Pore size distributions in hardened cement pastes with different degree of hydrations (0, 0.2, 0.4 0.6 and 0.8) at w/c ratios of (a) 0.3 (b) 0.4 and (c) 0.5.

4.3. Pore connectivity

Fig. 15 illustrates the continuous evolution of connectivity of capillary pore in cement pastes at w/c ratios of 0.3, 0.4 and 0.5 as time elapses. It can be seen that cement pastes at the w/cs of 0.3 and 0.4 can reach depercolation of capillary pore, while that at the w/c of 0.5 cannot. Moreover, the time of reaching depercolation at various w/cs is dramatically different. For example, the time of reaching depercolation in cement pastes at w/c=0.3 is several dozens of hours, by contrast, the depercolated time at w/c=0.4 is even a few hundreds of hours with one order of magnitude difference. In addition, from the tendency of curves of different shaped particles at the same w/c, the less equiaxed particles is positive to the connectivity of capillary pore. The time of reaching depercolation in cement pastes comprised of different shaped particles at the same w/c is various, but the difference of time is decreasing as w/c ratio decreases. For example, the time of depercolation in cement pastes made up of elongated-shaped particles at w/c=0.4 occurs at around 220 h, but this time occurs at 520 h for spherical particles, 300 h difference. However, this difference is retarded for w/c=0.3 with only 30 h.

To vividly visualize the depercolated process of capillary pores, the case of extracted pore networks in cement pastes consisting of spherical and elongated-shaped particles in accordance with that in Fig. 12 is shown in Fig. 16. Red voxels and blue voxels are connected and disconnected pores. It can be intuitively found that elongated-shaped particles can accelerate depercolation of capillary pore compared to spherical particles.

Fig. 17 shows the evolution of connectivity of capillary pores with DoH. It can be found that particle shapes have influence on the connectivity of capillary pores in hardened cement pastes. The less equiaxed cement particles are positive to depercolation of capillary pores, but this geometric effect of particle shapes is pretty slight. To directly correlate with capillary porosity, the evolution of connectivity of capillary pore is shown in Fig. 18. In Fig. 18, although the changing tendency of connectivity of capillary pore with porosity is different at low DoH due to the porosity difference and early local discrepancy of pore structure in 3D microstructure, the gradually same tendency will yet occur at a low porosity of around 0.25. Furthermore, the depercolated porosity of elongated-shaped particles at the same w/c is slightly superior to that of other shaped particles, which implies that the less equiaxed particles is beneficial to decreasing connectivity of capillary pores. In terms of depercolated capillary porosity, the values of all cement pastes are between 0.16 and 0.18 which are slightly smaller than inherent depercolation porosity of around 0.15 in CEMHYD3D model using digitalized spherical particles at resolution of 0.5 μm/voxel [31]. These all demonstrates that geometric effect of cement particles plays a weak role in depercolation process of capillary pores in cement pastes, while pore-to-solid ratio (porosity) is still the most pronounced influence factor to determine depercolation process.

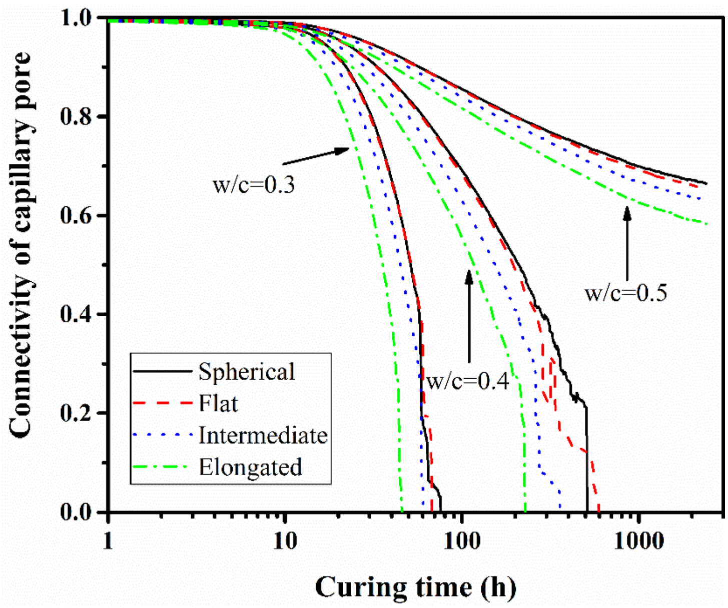

Fig. 15. Evolution of connectivity of capillary pore in simulated cement pastes against curing time.

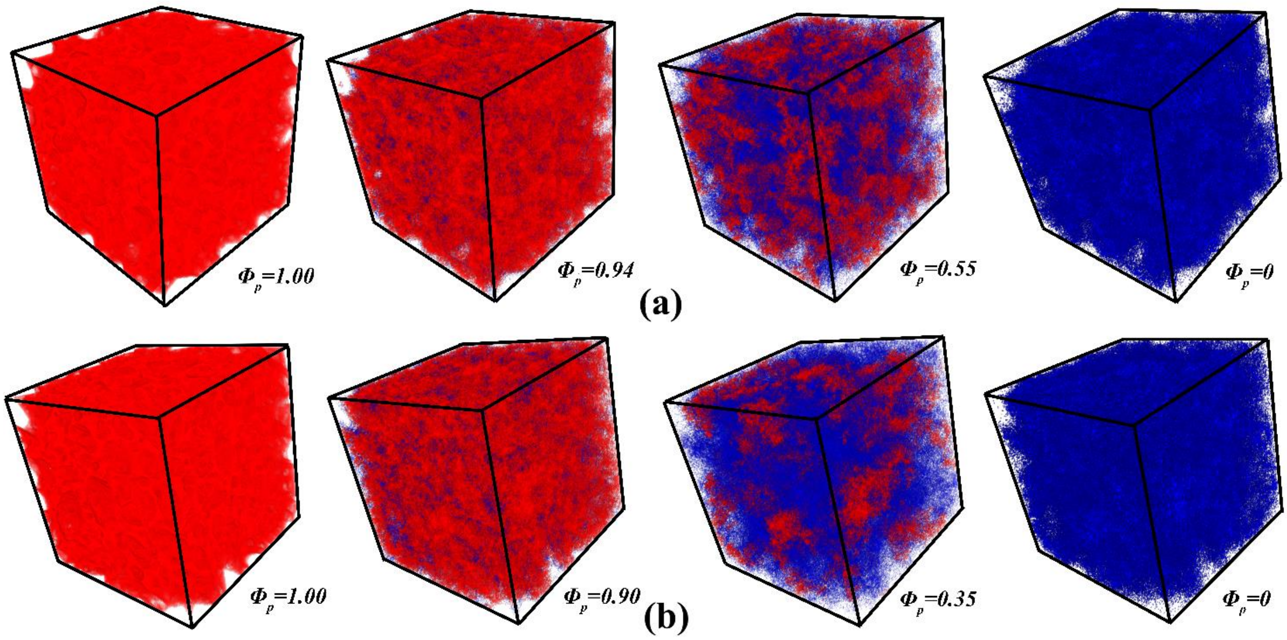

Fig. 16. 3D percolated (red) and depercolated pore structures (blue) in hardened cement pastes consisting of (a) spherical and (b) elongated-shaped particles at curing time of 0, 1, 7 and 28 d. $\boldsymbol{\Phi}_p$ means percolated capillary porosity.

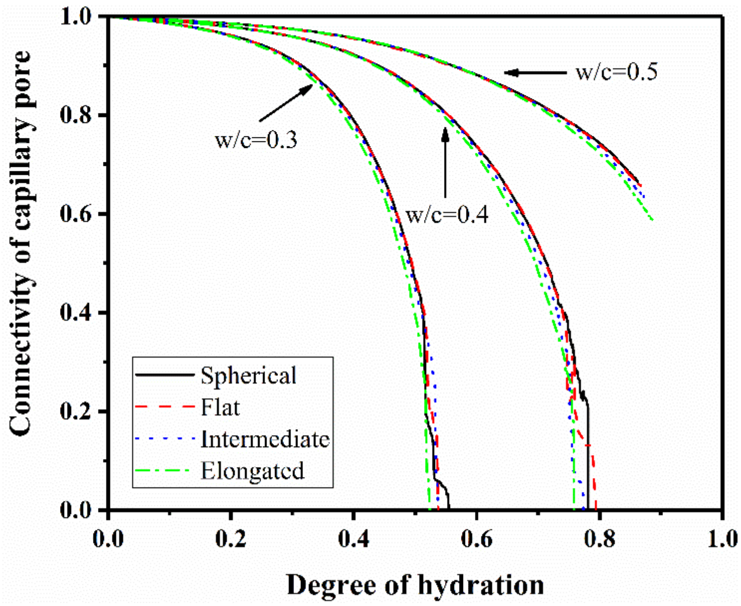

Fig. 17. Connectivity of capillary pore against degree of hydration.

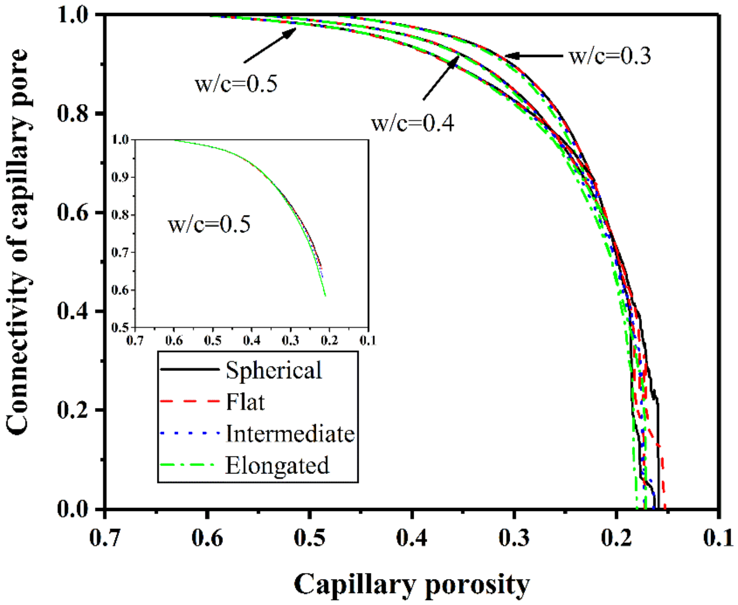

Fig. 18. Connectivity of capillary pore against capillary porosity.

4.4. Pore tortuosity

In order to achieve diffusion tortuosity of pore network in cement pastes, the program of random walk algorithm is implemented on these pore structures at the same curing time and degree of hydration, respectively. Mean square displacements in pore structures at curing time of 0, 1, 7 and 28 d for different shaped particles against time of lattice walk are illustrated in Fig. 19. It can be seen that as cement hydration proceeds, the slope of curve of mean square displacement against time of lattice of walk is decreasing, which means pore structures are becoming more tortuous. In Fig. 15, it can be concluded that capillary pores in cement pastes at curing age of 7 d and 28 d for w/c=0.3 and at curing age of 28 d for w/c=0.4 are disconnected. Therefore, the diffusion tortuosity of capillary pores is infinite in the corresponding simulated cement paste, which means mass transport properties are manipulated by porous C-S-H in this state [6, 44]. In addition, the difference of pore tortuosities in the initial packing microstructures is slight in spite of with the shaped discrepancy, which is in agreement with the finding that sand shaped effect has a weak influence on diffusivities in mortars consisting of various shaped aggregates [45]. Nevertheless, the shape-induced difference of pore tortuosity becomes much larger with cement hydration. The cement pastes made up of less equiaxed particles have larger pore tortuosity. With respect to the w/c ratio, cement pastes with a higher w/c ratio shows lower pore tortuosity. Based on Eq. (5), Fig. 20 illustrates the detailed values of pore tortuosity. It can be found that the cement pastes at a low w/c are more tortuous than that at a high w/c at the same curing age. It is also surprising to find that the values of pore tortuosity in the same microstructural process may even have two orders of magnitude difference, e.g., the microstructure at w/c=0.4 with values of tortuosity of around 1.5 at 0 d and around 200 at 7d shown in Fig 20 (b). This demonstrates that cement hydration process plays a decisive role in decreasing transport properties in cement pastes compared to cement particle packing.

Fig. 21 shows the detailed values of pore tortuosity in 3D pore network at DoHs of 0, 0.2, 0.4, 0.6 and 0.8 for different shaped particles. It can be found that only the cement pastes consisting of extremely less equiaxed particles, e.g., elongated-shaped particles, show considerable difference of pore tortuosity at the same DoH. However, shapes of cement powders in the real cement particles do not show extremely non-equiaxed attributes. Ref. [46] demonstrates that the average normalized length-to-width ratio is only between 1.27 and 1.46 for real cement particles. Herein, the length is defined as the largest-line surface point-to-surface point distance on the cement particle. The definition of width is satisfied with the largest-line surface point-to-surface point distance on the cement particle and the direction is perpendicular to the length as well. In terms of the numerical relationship between the normalized length-to-width ratio and principal moment of inertia of the particle used in this study, the square of normalized length-to-width ratio is approximately equal to the ratio of the maximum principal moment of inertia to the minimum principal moment of inertia [46]. After deduction, the average degree of irregularity of real cement particles is similar to the simulated intermediate-shaped particles with the average normalized length-to-width ratio of 1.41, but much smaller than elongated-shaped particles with the ratio of 2.08. Consequently, it can be concluded that particle shaped geometry of cement particles has slight effect on pore tortuosity in hardened cement pastes.

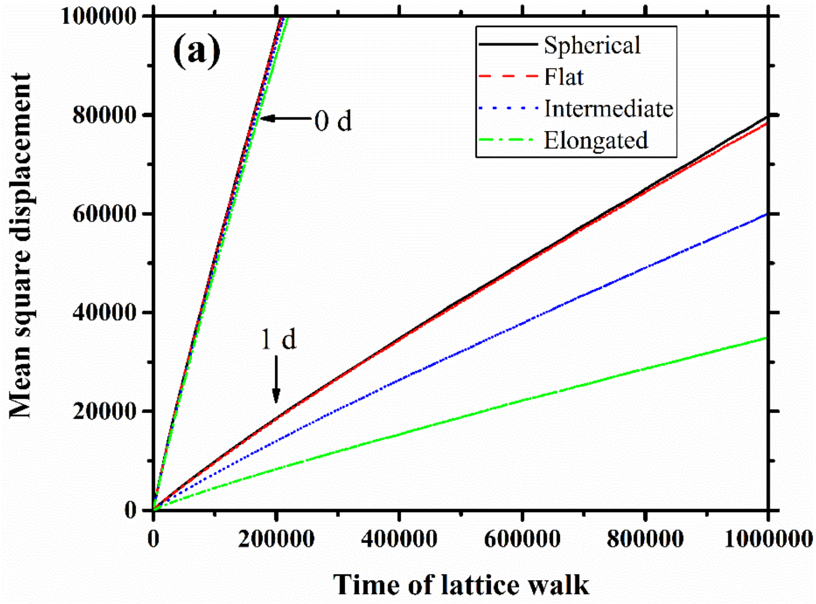
(a)
Mean square displacement
Time of lattice walk
0 d
1 d
Spherical
Flat
Intermediate
Elongated
0
20000
40000
60000
80000
100000
200000
400000
600000
800000
1000000

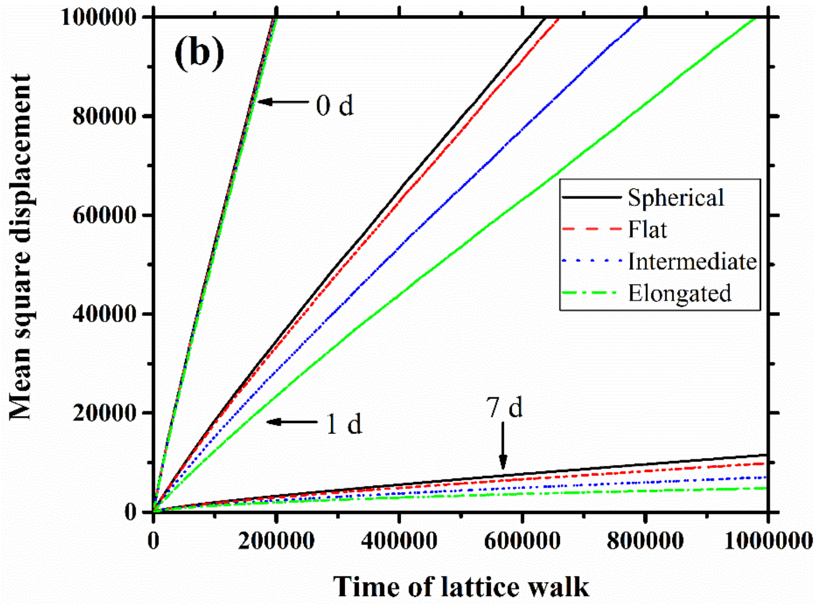
(b)
Mean square displacement
Time of lattice walk
0 d
1 d
7 d
Spherical
Flat
Intermediate
Elongated
0
20000
40000
60000
80000
100000
200000
400000
600000
800000
1000000

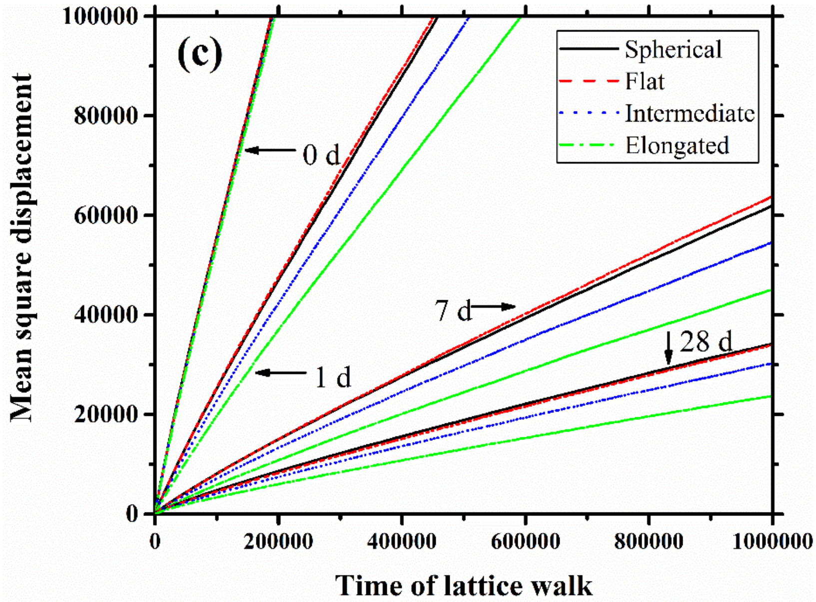

Fig. 19. Mean square displacement against time of lattice walk at w/c=0.3 (a), 0.4 (b) and 0.5 (c).

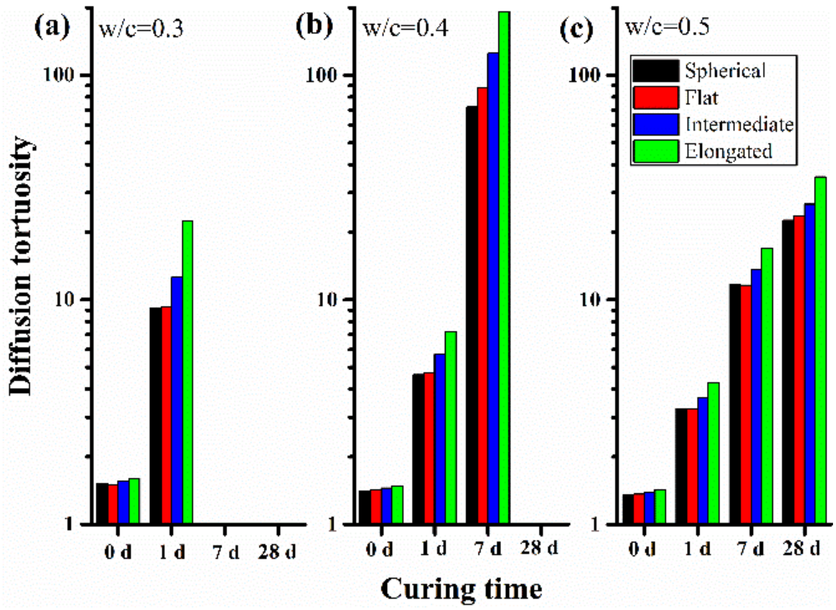

Fig. 20. Diffusion tortuosity in hardened cement pastes against curing time.

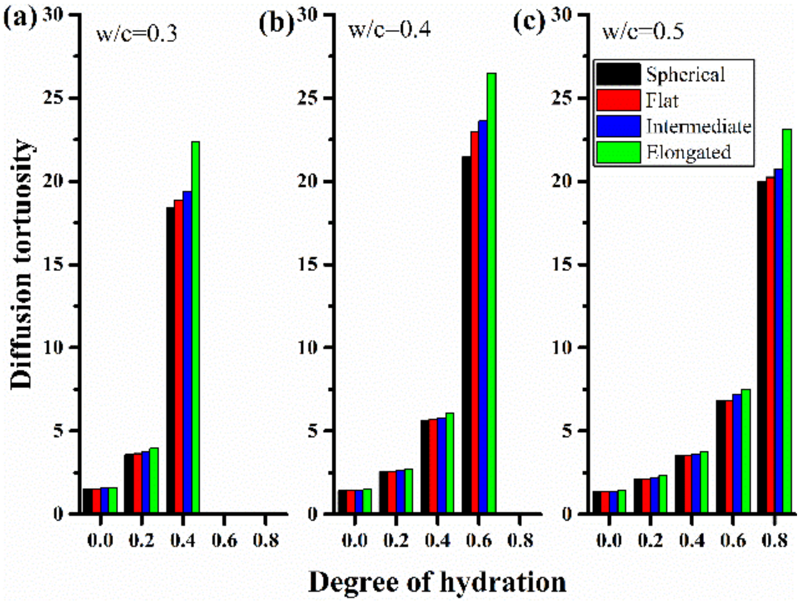

Fig. 21. Diffusion tortuosity in hardened cement pastes against degree of hydration.

5. Conclusions

In this paper, the effects of cement particle shapes on capillary pore structures in hardened cement pastes are investigated in detail, which is simulated using a discrete-based hydration model. Some algorithms along with home-made programs for determining 3D pore structure parameters including porosity, pore size distribution, pore connectivity and pore tortuosity, are carried out on the simulated cement pastes consisting of different particles with representative irregular shapes. Based on the findings of this study, the following conclusions can be drawn:

- Cement particle shapes have considerable effects on pore structure parameters in cement pastes at the early curing age, while this effect will decrease as time elapses. Due to high area surface, the less equiaxed cement particles can contribute to cement hydration, which leads to corresponding hardened cement pastes with less porosity, smaller pore size, faster pore depercolation and more tortuosity in the early curing period, compared to equiaxed ones. Meanwhile, large water-to-cement ratio is beneficial to extending this effect resulting from surface area difference of cement particles to some degree.
- Besides the dramatic influence factor, surface area of cement particles, the less considered geometric attribute of irregular shaped particle also plays a slight role in pore structure parameters in cement pastes. The less equiaxed particle is positive to decreasing pore size, accelerating capillary pore depercolation process and increasing pore tortuosity. However, the geometric attribute of cement particles generally shows a weak

influence on the evolution of pore structures in cement pastes overall. Consequently, pore network is rather similar for each cement particle shape, which indicating that the cement particle shape will have no significant influence on the service life of reinforced concrete structures.

Acknowledgments

The financial support from National Natural Science Foundation of China (No. 51378116, No. 51678143 and NO. 51408597), Ministry of Science and Technology of China (973 Program, No. 2015CB655102) and China Scholarship Council (CSC) are gratefully acknowledged. The authors also would like to thank Dr. Dale Bentz from the National Institute for Standards and Testing, USA, for kindly providing the source codes of CEMHYD3D model.

Reference

[1] H. Ma, Z. Li, Realistic pore structure of Portland cement paste: experimental study and numerical simulation, Computers and Concrete 11(4) (2013) 317-336.

[2] Z. Liu, W. Chen, Y. Zhang, H. Lv, A three-dimensional multi-scale method to simulate the ion transport behavior of cement-based materials, Construction and Building Materials 120 (2016) 494-503.

[3] Q. Huang, Z. Jiang, X. Gu, W. Zhang, B. Guo, Numerical simulation of moisture transport in concrete based on a pore size distribution model, Cement and Concrete Research 67 (2015) 31-43.

[4] S. Mindess, J.F. Young, D. Darwin, Concrete, Prentice Hall2003.

[5] W.-Y. Kuo, J.-S. Huang, C.-H. Lin, Effects of organo-modified montmorillonite on strengths and permeability of cement mortars, Cement and Concrete Research 36(5) (2006) 886-895.

[6] Y. Zhang, C. Liu, Z. Liu, G. Liu, L. Yang, Modelling of diffusion behavior of ions in low-density and high-density calcium silicate hydrate, Construction and Building Materials 155 (2017) 965-980.

[7] K. Ishizaki, S. Komarneni, M. Nanko, Porous Materials: Process technology and applications, Springer Science and Business Media 2013.

[8] P. Chindaprasirt, C. Jaturapitakkul, T. Sinsiri, Effect of fly ash fineness on compressive strength and pore size of blended cement paste, Cement and Concrete Composites 27(4) (2005) 425-428.

[9] P. Chindaprasirt, C. Jaturapitakkul, T. Sinsiri, Effect of fly ash fineness on microstructure of blended cement

paste, Construction and Building Materials 21(7) (2007) 1534-1541.

[10] S. Tsivilis, E. Chaniotakis, G. Batis, C. Meletiou, V. Kasselouri, G. Kakali, A. Sakellariou, G. Pavlakis, C. Psimadas, The effect of clinker and limestone quality on the gas permeability, water absorption and pore structure of limestone cement concrete, Cement and Concrete Composites 21(2) (1999) 139-146.

[11] E.J. Garboczi, J.W. Bullard, Shape analysis of a reference cement, Cement and Concrete Research 34(10) (2004) 1933-1937.

[12] S. Erdoğan, X. Nie, P.E. Stutzman, E.J. Garboczi, Micrometer-scale 3-D shape characterization of eight cements: Particle shape and cement chemistry, and the effect of particle shape on laser diffraction particle size measurement, Cement and Concrete Research 40(5) (2010) 731-739.

[13] J.W. Bullard, E.J. Garboczi, A model investigation of the influence of particle shape on portland cement hydration, Cement and Concrete Research 36(6) (2006) 1007-1015.

[14] D.P. Bentz, Quantitative comparison of real and CEMHYD3D model microstructures using correlation functions, Cement and Concrete Research 36(2) (2006) 259-263.

[15] L. Holzer, B. Muench, M. Wegmann, P. Gasser, R.J. Flatt, FIB‐Nanotomography of Particulate Systems—Part I: Particle Shape and Topology of Interfaces, Journal of the American ceramic society 89(8) (2006) 2577-2585.

[16] K. Van Breugel, Numerical simulation of hydration and microstructural development in hardening cement-based materials (I) theory, Cement and Concrete Research 25(2) (1995) 319-331.

[17] S. Bishnoi, K.L. Scrivener, μic: A new platform for modelling the hydration of cements, Cement and Concrete Research 39(4) (2009) 266-274.

[18] W. Xu, H. Chen, Microstructural characterization of fresh cement paste via random packing of ellipsoidal cement particles, Materials Characterization 66 (2012) 16-23.

[19] W. Xu, H. Chen, Numerical investigation of effect of particle shape and particle size distribution on fresh cement paste microstructure via random sequential packing of dodecahedral cement particles, Computers and Structures 114 (2013) 35-45.

[20] C. Liu, R. Huang, Y. Zhang, Z. Liu, M. Zhang, Modelling of irregular-shaped cement particles and microstructural development of Portland cement, Construction and Building Materials 168 (2018) 362-378.

[21] X. Jia, R. Williams, A packing algorithm for particles of arbitrary shapes, Powder technology 120(3) (2001) 175-186.

[22] M. Zhang, Y. He, G. Ye, D.A. Lange, K. van Breugel, Computational investigation on mass diffusivity in Portland cement paste based on X-ray computed microtomography (μCT) image, Construction and Building Materials 27(1) (2012) 472-481.

[23] Y. Gao, G. De Schutter, G. Ye, H. Huang, Z. Tan, K. Wu, Characterization of ITZ in ternary blended cementitious composites: experiment and simulation, Construction and building Materials 41 (2013) 742-750.

[24] D.P. Bentz, E.J. Garboczi, Percolation of phases in a three-dimensional cement paste microstructural model, Cement and Concrete Research 21(2-3) (1991) 325-344.

[25] D.P. Bentz, G. Sant, J. Weiss, Early-age properties of cement-based materials. I: Influence of cement fineness, Journal of Materials in Civil Engineering 20(7) (2008) 502-508.

[26] D.P. Bentz, Three‐Dimensional Computer Simulation of Portland Cement Hydration and Microstructure Development, Journal of the American Ceramic Society 80(1) (1997) 3-21.

[27] D.P. Bentz, E.J. Garboczi, C.J. Haecker, O.M. Jensen, Effects of cement particle size distribution on performance properties of Portland cement-based materials, Cement and Concrete Research 29(10) (1999) 1663-1671.

[28] M.A.B. Promentilla, T. Sugiyama, T. Hitomi, N. Takeda, Quantification of tortuosity in hardened cement pastes using synchrotron-based X-ray computed microtomography, Cement and Concrete Research 39(6) (2009) 548-557.

[29] P. Navi, C. Pignat, Simulation of cement hydration and the connectivity of the capillary pore space, Advanced Cement Based Materials 4(2) (1996) 58-67.

[30] E. Gallucci, K. Scrivener, A. Groso, M. Stampanoni, G. Margaritondo, 3D experimental investigation of the microstructure of cement pastes using synchrotron X-ray microtomography (μCT), Cement and Concrete Research 37(3) (2007) 360-368.

[31] E.J. Garboczi, D.P. Bentz, The effect of statistical fluctuation, finite size error, and digital resolution on the phase percolation and transport properties of the NIST cement hydration model, Cement and Concrete Research 31(10) (2001) 1501-1514.

[32] P. Halamickova, R.J. Detwiler, D.P. Bentz, E.J. Garboczi, Water permeability and chloride ion diffusion in Portland cement mortars: relationship to sand content and critical pore diameter, Cement and concrete research 25(4) (1995) 790-802.

[33] R. Kumar, B. Bhattacharjee, Assessment of permeation quality of concrete through mercury intrusion porosimetry, Cement and Concrete Research 34(2) (2004) 321-328.

[34] D. Manmohan, P. Mehta, Influence of pozzolanic, slag, and chemical admixtures on pore size distribution and permeability of hardened cement pastes, Cement, Concrete and Aggregates 3(1) (1981) 63-67.

[35] B. Münch, L. Holzer, Contradicting geometrical concepts in pore size analysis attained with electron microscopy and mercury intrusion, Journal of the American Ceramic Society 91(12) (2008) 4059-4067.

[36] H. Dong, P. Gao, G. Ye, Characterization and comparison of capillary pore structures of digital cement pastes, Materials and Structures 50(2) (2017) 154.

[37] M.A.B. Promentilla, S.M. Cortez, R.A.D. Papel, B.M. Tablada, T. Sugiyama, Evaluation of microstructure and transport properties of deteriorated cementitious materials from their X-ray computed tomography (CT) images, Materials 9(5) (2016) 388.

[38] B. Ghanbarian, A.G. Hunt, R.P. Ewing, M. Sahimi, Tortuosity in porous media: a critical review, Soil science society of America journal 77(5) (2013) 1461-1477.

[39] W.B. Lindquist, S.M. Lee, D.A. Coker, K.W. Jones, P. Spanne, Medial axis analysis of void structure in three‐dimensional tomographic images of porous media, Journal of Geophysical Research: Solid Earth 101(B4) (1996) 8297-8310.

[40] N.O. Shanti, V.W. Chan, S.R. Stock, F. De Carlo, K. Thornton, K.T. Faber, X-ray micro-computed tomography and tortuosity calculations of percolating pore networks, Acta Materialia 71 (2014) 126-135.

[41] J. Montes, F. Cuevas, J. Cintas, Electrical and thermal tortuosity in powder compacts, Granular Matter 9(6) (2007) 401-406.

[42] S. Pardo-Alonso, J. Vicente, E. Solórzano, M.Á. Rodriguez-Perez, D. Lehmhus, Geometrical tortuosity 3D calculations in infiltrated aluminium cellular materials, Procedia Materials Science 4 (2014) 145-150.

[43] Y. Nakashima, S. Kamiya, Mathematica programs for the analysis of three-dimensional pore connectivity and anisotropic tortuosity of porous rocks using X-ray computed tomography image data, Journal of Nuclear

Science and Technology 44(9) (2007) 1233-1247.

[44] E. Garboczi, D. Bentz, Computer simulation of the diffusivity of cement-based materials, Journal of materials science 27(8) (1992) 2083-2092.

[45] S.D. Abyaneh, H. Wong, N. Buenfeld, Modelling the diffusivity of mortar and concrete using a three-dimensional mesostructure with several aggregate shapes, Computational Materials Science 78 (2013) 63-73.

[46] L. Holzer, R.J. Flatt, S.T. Erdoğan, J.W. Bullard, E.J. Garboczi, Shape comparison between 0.4–2.0 and 20–60 μm cement particles, Journal of the American Ceramic Society 93(6) (2010) 1626-1633.